Subsurface Nanoimaging by THz Pulse Near-Field Microscopy

Kiwon Moon, Hongkyu Park, Jeonghoi Kim, Youngwoong Do, Soonsung Lee, Gyuseok Lee, Hyeona Kang, Jin-Woo Kim†, and HAEWOOK HAN*
Department of Electrical and Computer Engineering, POSTECH, Pohang, Gyeongbuk 790-784, Korea
†Department of Biological and Agricultural Engineering, University of Arkansas, Fayetteville, AR 72701, USA

***Abstract*—Combined with THz time-domain spectroscopy, THz near-field microscopy based on an atomic force microscope is a technique that, while challenging to implement, is invaluable for probing low-energy light-matter interactions of solid-state and biomolecular nanostructures, which are usually embedded in background media. Here, we experimentally demonstrate a broadband THz pulse near-field microscope that provides subsurface nanoimaging with a nearly frequency-independent lateral resolution of 90 nm, corresponding to ~λ/3300 at 1 THz.**

I. INTRODUCTION

Terahertz time-domain spectroscopy (THz-TDS) has recently been a powerful tool for probing fundamental low-energy dynamic processes in solid-state materials and devices. Understanding such low-energy THz dynamics has become crucial for developing next-generation electronic and optical devices. To realize THz-TDS with subwavelength resolution, various types of near-field imaging techniques have been combined with THz-TDS. Nanoscale near-field imaging in the terahertz (THz) spectral range is of great importance for studying intriguing phenomena such as biomolecular vibrations and carrier dynamics in quantum-confined nanostructures.

Conventional THz time-domain spectroscopy can provide macroscopic imaging averaged over an ensemble of such nanostructures. Their spatial resolutions are, however, limited to ~λ/2 by diffraction. Therefore, several types of THz pulse scanning near-field optical microscopes (SNOMs) have been developed to achieve sub-wavelength resolutions [1–9]. In contrast to visible or IR SNOMs, most THz SNOMs have been based on THz pulse TDS systems [1–8], making it possible to perform ultra-broadband THz spectroscopy. Among the THz SNOM systems, the scattering-type SNOM (s-SNOM) has been the most successful technique so far [6–13].

In the THz s-SNOM, the scattered field from the tip apex is measured in the far-field region. Sub-micrometer resolutions are enabled by the strongly localized near-field around the probe tip [14]. Thus, it is essential to understand the near-field interaction in the tip-substrate system, and there have been several analytic models [15–18] and also numerical simulations [19,20] to solve the problems. The most popular approach has been the point dipole image method (PDIM) [8–12] where the probe tip is replaced by a polarizable *point* dipole [10]. Because of its simplicity, the PDIM has been widely used to analyze experimental data [8–12], and has provided qualitative understanding on several important aspects of the s-SNOM, including resolution [10] and optical phase contrast [11]. However, because the boundary conditions are not matched on the surface of the probe sphere, the PDIM becomes incorrect as the sphere approaches the substrate [15–18]. We have recently developed a self-consistent line dipole image method (LDIM) based on an exact quasi-electrostatic image theory [21–23] for the analysis of THz s-SNOMs. The accuracy of the LDIM was verified by a quantitative comparison with numerical simulations based on the finite element method (FEM). The experimental approach curves and contrasts of THz s-SNOMs were in excellent agreement with the LDIM calculations.

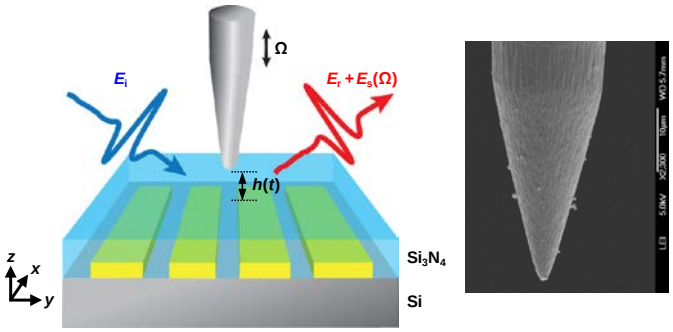

Fig. 1. Schematic of THz s-SNOM system with a tungsten nanoprobe.

At present, scattering-type scanning near-field optical microscopy (s-SNOM) seems to be the most viable technique that can offer nanoscale resolution and broadband THz spectroscopy simultaneously. In this work, we report a broadband subsurface nanoimaging by a THz pulse s-SNOM system that has recently been developed by combining a homemade tapping-mode AFM and a conventional THz-TDS system [24].

II. EXPERIMENTS AND RESULTS

Using off-axis parabolic mirrors, the incident THz pulse was focused on an AFM probe, and focused on a THz photoconductive antenna to measure the far-field as shown in Fig. 1. For the nanoscale resolution we fabricated a tungsten probe with an apex diameter of less than 100 nm by using an electrochemical etching method. The THz s-SNOM system is shown in Fig. 1. The total electric field at the probe tip is the sum of the incident field, the specularly reflected field at the sample surface, and the scattered field that includes all the information about near-field interaction. The scattered field is a nonlinear function of the probe-sample distance, and thus the scattered field is the sum of the harmonics of the dithering frequency (Ω). To extract the scattered field from the total field, the n^{th}-harmonic component (E_n) of the photocurrent in the THz antenna was measured by demodulation at $n\Omega$. We used a metallic grating embedded in a dielectric layer. A 30 nm thick gold grating with a period of 800 nm was fabricated on an insulating Si substrate using holographic lithography followed by e-beam evaporation. After depositing a Si_3N_4 layer, the sample surface was flattened using a chemical-mechanical polishing process.

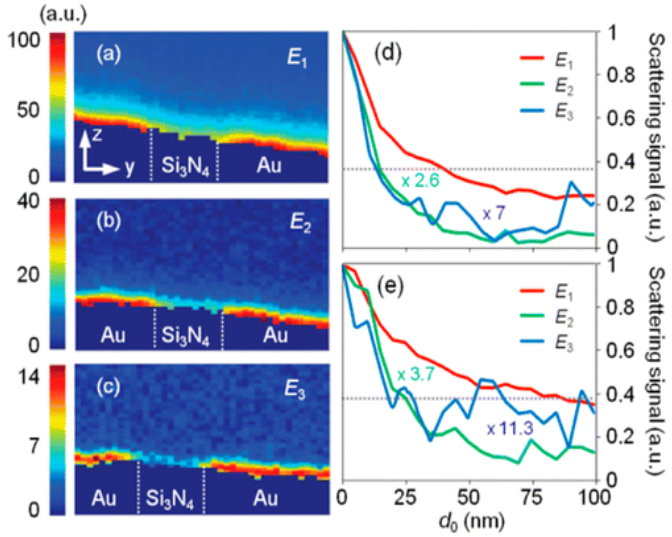

Fig. 2 Peak intensity images from approach curves above the sample surface. (a) E_1, (b) E_2, and (c) E_3 (d,e) approach curves on the Au and Si sections. The size of the images is 800 nm by 200 nm. The interaction distances were 38 nm (88 nm), 15 nm (26 nm), and 13 nm (18 nm) for E_1, E_2, and E_3, respectively, where the dotted lines shows the e^{-1} levels relative to the maximum signals.

The line-scan images is shown in Fig. 2 for the peak intensities of scattered fields using the approach curves of E_1, E_2, and E_3 where the subsurface grating depth was ~30 nm. The depth of the gold grating varied over the sample surface, and moving to a position with a thicker Si_3N_4 layer resulted in a slightly reduced image contrast. It should be noted that the multiple reflections due to the multilayer sample structures were not observed because the depth of the grating was much smaller than the THz wavelength. The scattered signal only became significant when the probe was near the surface, which is clear evidence of near-field interaction. We also measured the probe-sample interaction distance at which the signal reduced to $1/e$ with respect to the maximum signal, which means that clear near-field imaging is possible only when the probe-to-sample distance is shorter than the interaction distance. Above the Au (Si) section, the interaction lengths measured from the line-scan images were 38 nm (88 nm), 15 nm (26 nm), and 13 nm (18 nm) for E_1, E_2, and E_3, respectively. The near-field imaging contrast decreased with increasing demodulation order. If the resolution is important, E_2 and E_3 may be preferred to E_1. However, for subsurface imaging with a thick coating layer, E_1 seems to be the reasonable choice because the interaction distance is much longer than the high-order demodulations.

The near-field peak intensity images of E_1, E_2, and E_3, along with the AFM topographic image, are shown in Fig. 2(a). Because of the polishing process, no sign of the subsurface grating structure was observed in the AFM image. However, in the near-field images the metallic grating under the flat surface was clearly revealed. The subsurface lateral resolutions were estimated to be 90, 90, and 80 nm for E_1, E_2, and E_3, respectively. The spatiotemporal and spatio-spectral images are shown in Fig. 2(b). The spatio-spectral image of $E_1(x, \omega)$ was obtained from the Fourier transformation of $E_1(x, t_d)$. The lateral resolution of the spatio-spectral image was also nearly frequency-independent, which has not been achieved with THz s-SNOM.

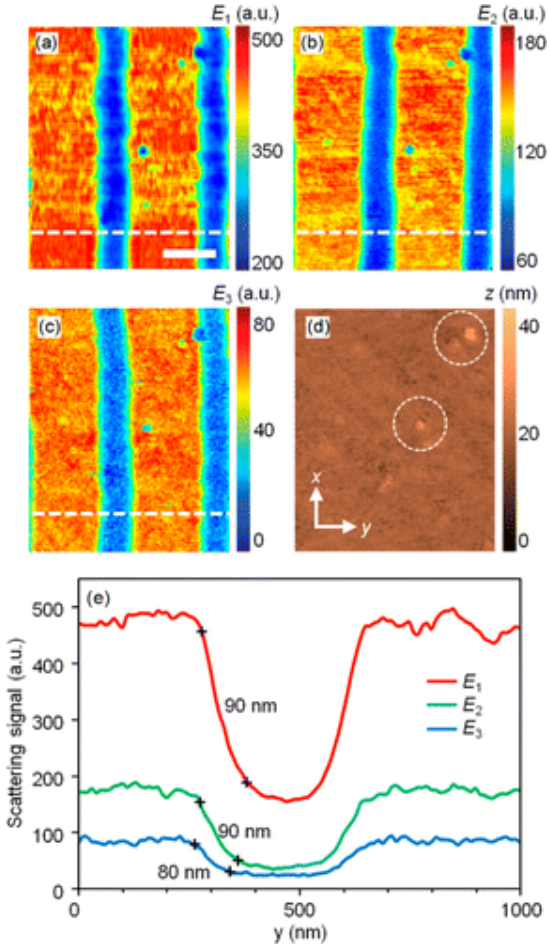

Fig. 3 THz near-field peak intensity images for (a) E_1, (b) E_2, (c) E_3, and (d) AFM topography, where the scale bar is 500 nm. (e) Near-field profiles along the dashed lines in (a–c), where the blue, green, and red curves represent E_1, E_2, and E_3, respectively. Topographic artifacts are observed at surface protrusions marked with dashed circles.

Figure 3 shows the near-field peak intensity images of E_1, E_2, and E_3, along with the AFM topographic image. Because of the polishing process, no sign of the subsurface grating structure was observed in the AFM image. However, in the near-field images the metallic grating under the flat surface was clearly revealed. The subsurface lateral resolutions were estimated to be 90, 90, and 80 nm for E_1, E_2, and E_3, respectively. The small spatial offsets in the E_1, E_2, and E_3 images are due to the long-term drift of the nanostage during the measurements. In the AFM image, we observed small protrusions, being clearly imaged in the near-field images, as well. The protrusions are due to the silica residuals of the polishing process. With these protrusions, the resolution is better than 40 nm, but this is a result of the surface topography rather than an effect of constituent material. Therefore, we ignore the protrusions and conclude that the resolution of our THz s-SNOM is ~90 nm for the near-field imaging. In general, the scattered signal intensity strongly depends not only on d_0 but also on the local surface profile and the material distribution. Even tiny nanometer-sized surface protrusions can cause large changes in the scattering signal, leading to topographical artifacts. Therefore, for near-field imaging of nanostructures we need to precisely control the probe-sample distance using an AFM system.

III. SUMMARY

We have successfully demonstrated subsurface broadband THz pulse near-field imaging of an embedded metallic grating. The lateral resolution of the first-order demodulation was ~90 nm, which is nearly frequency-independent, and is comparable to those of the second- and third-order demodulations. We also defined and measured the probe-sample interaction length, which is a measure of the strength of the probe-sample interaction, to determine the depth limit of subsurface near-field imaging.

It seems that the first-order demodulation is preferred to higher-order demodulations for subsurface nanoscale imaging, particularly for nanostructures embedded in thick films because the first-order demodulation has the longest interaction length, and a lateral resolution comparable to the higher-order demodulation. We expect that subsurface broadband THz near-field imaging will become an important tool for studying THz dynamics in nanoscale devices and nanomaterials because many of these nanostructures are embedded in host materials.

REFERENCES

[1] S. Hunsche, M. Koch, I. Brener, and M. C. Nuss, "THz near-field imaging," Opt. Commun., Vol. 150, no. 1-6, pp. 22–26, 1998.

[2] Q. Chen and X.-C. Zhang, "Semiconductor dynamic aperture for near-field terahertz wave imaging," IEEE J. Sel. Top. Quantum Electron., Vol. 7, no. 4, pp. 608–614, 2001.

[3] N. C. J. van der Valk and P. C. M. Planken, "Electro-optic detection of subwavelength terahertz spot sizes in the near field of a metal tip," Appl. Phys. Lett., vol. 81, no. 9, pp. 1558–1560, 2002.

[4] T. Yuan, H. Park, J. Xu, H. Han, and X.-C. Zhang, "Field induced THz wave emission with nanometer resolution," Proc. SPIE, vol. 5649, pp. 1–8, 2005.

[5] H. T. Chen, R. Kersting, and G. C. Cho, "Terahertz imaging with nanometer resolution," Appl. Phys. Lett., vol. 83, no. 15, pp. 3009–3011, 2003.

[6] H. Park, J. Kim, and H. Han, "THz pulse near-field microscope with nanometer resolution," 35th Workshop: Physics and Technology of THz Photonics 2005, Erice, Italy, pp. 20–26, Jul. 2005.

[7] H. Park, J. Kim, M. Kim, H. Han, and I. Park, "Terahertz near-field microscope," Joint 31st International Conference on Infrared Millimeter Waves and 14th International Conference on Terahertz Electronics (IRMMW-THz 2006), Shanghai, China, pp. 18–22 Sep. 2006.

[8] 8. H.-G. von Ribbeck, M. Brehm, D. W. van der Weide, S. Winnerl, O. Drachenko, M. Helm, and F. Keilmann, "Spectroscopic THz near-field microscope," Opt. Express 16(5), 3430–3438 (2008).

[9] A. J. Huber, F. Keilmann, J. Wittborn, J. Aizpurua, and R. Hillenbrand, "Terahertz near-field nanoscopy of mobile carriers in single semiconductor nanodevices," Nano Lett. Vol. 8, no. 11, pp. 3766–3770, 2008.

[10] B. Knoll and F. Keilmann, "Enhanced dielectric contrast in scattering-type scanning near-field optical microscopy," Opt. Commun., vol. 182, vol. 4-6, pp. 321–328, 2000.

[11] R. Hillenbrand and F. Keilmann, "Complex optical constants on a subwavelength scale," Phys. Rev. Lett., vol. 85, no. 14, pp. 3029–3032, 2000.

[12] T. Taubner, R. Hillenbrand, and F. Keilmann, "Nanoscale polymer recognition by spectral signature in scattered infrered near-field microscopy," Appl. Phys. Lett., vol. 85, no. 21, pp. 5064–5066, 2004.

[13] M. Labardi, S. Patanè, and M. Allegrini, "Artifact-free near-field optical imaging by apertureless microscopy," Appl. Phys. Lett., vol. 77, no. 5, pp. 621–623, 2000.

[14] L. Novotny, R. X. Bian, and X. S. Xie, "Theory of nanometric optical tweezers," Phys. Rev. Lett., vol. 79, no. 4, pp. 645–648, 1997.

[15] P. K. Aravind and H. Metiu, "The effects of the interaction between resonances in the electromagnetic response of a sphere-plane structure: applications to surface enhanced spectroscopy," Surf. Sci., vol. 124, no. 2-3, pp. 506–528, 1983.

[16] S. V. Sukhov, "Role of multipole moment of the probe in apertureless near-field optical microscopy," Ultramicroscopy, vol. 101, no. 2-4, pp. 111–122, 2004.

[17] J. A. Porto, P. Johansson, S. P. Apell, and T. López-Ríos, "Resonance shift effects in apertureless scanning near-field optical microscopy," Phys. Rev. B, vol. 67, no. 8, pp. 085409, 2003.

[18] A. Cvitkovic, N. Ocelic, and R. Hillenbrand, "Analytical model for quantitative prediction of material contrasts in scattering-type near-field optical microscopy," Opt. Express, vol. 5, no. 14, pp. 8550–8565, 2007.

[19] R. Esteban, R. Vogelgesang, and K. Kern, "Tip-substrate interaction in optical near-field microscopy," Phys. Rev. B 75(19), 195410 (2007).

[20] M. Brehm, A. Schliesser, F. Čajko, I. Tsukerman, and F. Keilmann, "Antenna-mediated back-scattering efficiency in infrared near-field microscopy," Opt. Express, vol. 16, no. 15, pp. 11203–11215, 2008.

[21] I. V. Lindell, M. E. Ermutlu, and A. H. Sihvola, "Electrostatic image theory for layered dielectric sphere," IEE Proc., H Microw. Antennas Propag. vol. 139, no. 2, pp.186–192, 1992.

[22] I. V. Lindell, J. C.-E. Sten, and K. I. Nikoskinen, "Electrostatic image method for the interaction of two dielectric spheres," Radio Sci., vol. 28, no. 3, pp. 319–329, 1993.

[23] K. Moon, J. Kim, Y. Han, H. Park, E. Jung, and H. Han, "Iterative image method for apertureless THz near-field microscope," presented at the IRMMW-THz 2008, Caltech, California, USA, pp. 15–19, Sept. 2008.

[24] Kiwon Moon, Hongkyu Park, Jeonghoi Kim, Youngwoong Do, Soonsung Lee, Gyuseok Lee, Hyeona Kang, and Haewook Han, "Subsurface nanoimaging by broadband terahertz pulse near-field microscopy," nano. Lett., vol. 15, no. 1, pp. 549–552, 2015.